A New Method of Current Switching for Linear Wide-Range Measurement Systems

Eduardo Winston Pontes and Ademar Ferreira, *Member, IEEE*

***Abstract*—This new and general method here called overflow current switching allows a fast, continuous, and smooth transition between scales in wide-range current measurement systems, like electrometers. This is achieved, using a hydraulic analogy, by diverting only the overflow current, such that no slow element is forced to change its state during the switching. As a result, this approach practically eliminates the long dead time in low-current (picoamperes) switching. Similar to a logarithmic scale, a composition of n adjacent linear scales, like a segmented ruler, measures the current. The use of a linear wide-range system based on this technique assures fast and continuous measurement in the entire range, without blind regions during transitions and still holding suitable accuracy for many applications. A full mathematical development of the method is given. Several computer realistic simulations demonstrated the viability of the technique.**

***Index Terms*—Fast electrometers, linear electrometers, low-current switching, wide-range current measurement, wide-range electrometers.**

I. Introduction

WIDE-RANGE current measurements have been normally performed by the use of logarithmic amplifiers like that described in [1] or by switching scales on linear amplifiers [2]–[5]. The choice of one or the other is based on the application. When accuracy is not the main factor and a continuous and smooth measurement without dead time is desirable, the logarithmic amplifier can be a good choice. On the other hand, when accuracy is the primary factor, a linear approach is preferable.

Wide-range current measurement is extensively used in many fields, such as in nuclear science [6], [7], where ranges from picoamperes (or fractions) up to few milliamperes are common. In certain cases, the most demanding applications require monitoring a variable continuously and accurately in an extended range of many decades, without blind regions during transitions, and with a good time response. Switching current near the picoampere range, however, implies long dead time (seconds) caused by large-time-constant transients, which are characteristic of the circuits operating in these conditions. This factor therefore suggests not using traditional switching for these particular purposes. Considering this fact, this work seeks to combine in a single concept the advantages of the linear and logarithmic systems, i.e., continuous monitoring, appropriate time response, and suitable accuracy, as applicable to certain wide-range measurement systems, like electrometers. In this way, it pursues a different goal from certain approaches, such as those in [1]–[8], and from other specific techniques, like that in [9]. Also, different from a recent work [10], our work aims at using a new general methodology and development for that purpose.

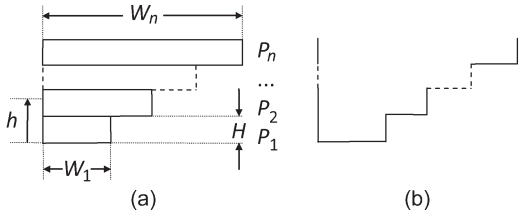

Fig. 1. Cross sections of (a) a vertical stack of pipes and (b) a gutter. The direction of the fluid stream is perpendicular to the plane of this page.

This paper is organized as follows: Section II presents the general concept of the method, Section III shows how to apply this concept for the purpose of building an overflow current switching (OCS) measurement system, Section IV focuses on the corresponding processing alternatives, Section V deals with some design considerations, and Section VI performs a simulated application for the purpose of demonstrating the method.

II. Concept of the Method

The concept of the OCS method can be better understood by making use of a hydraulic analogy as next described.

Let us consider a set of rectangular section pipes $(P_1, P_2, \ldots, P_n)$ having the same height (H) but different widths $(W_1, W_2, \ldots, W_n)$, *vertically stacked* as shown in Fig. 1(a). This arrangement is connected to a gutter [Fig. 1(b)] having the same cross-sectional profile, so that a fluid stream of constant speed in the gutter, representing the electric current to be measured, can be smoothly directed to the pipes.

Note that each pipe has different limits (section area or scale) for the fluid flow. For a small fluid flow i, only pipe P_1 is being used, i.e., is *active*, at a height (potential) h_1. Increasing the flow continuously, its potential increases proportionally until threshold H is reached. Increasing a little more, the overflow diverts to pipe P_2, proportionally increasing its potential h_2 from zero up to H. The sequence continues until the last pipe

Manuscript received February 14, 2011; revised May 27, 2011; accepted July 19, 2011. Date of publication October 18, 2011; date of current version January 5, 2012. The Associate Editor coordinating the review process for this paper was Dr. Theodore Laopoulos.

E. W. Pontes is with the Instituto de Pesquisas Energéticas e Nucleares, Comissão Nacional de Energia Nuclear, São Paulo 05508-000, Brazil (e-mail: ewpontes@ipen.br).

A. Ferreira is with the Departamento de Engenharia de Telecomunicações e Controle, Universidade de São Paulo, São Paulo 05508-900, Brazil (e-mail: ademar@lac.usp.br).

Digital Object Identifier 10.1109/TIM.2011.2169181

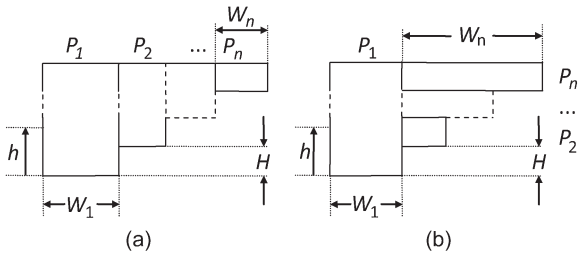

Fig. 2. Cross sections of two stacks of pipes: (a) Horizontal and (b) hybrid H^1V (one horizontal and $n-1$ vertical) configurations. The gutter is the same as that in Fig. 1(b).

P_n becomes active and reaches full scale. Reducing the flow, the process is inverted.

This procedure provides a smooth and fast switching between two adjacent pipes (scales), practically without transient, compared to a traditional switching mode where a pipe would be replaced by the next, resulting in a large and slow transient.

Proceeding with our analogy, let us now develop some quantitative analysis. Consider in Fig. 1(a) the last pipe to become active, for example, P_η. It conducts a flow proportional to the potential h_η $(0 < h_\eta \leq H)$, and the $\eta - 1$ previous pipes are fully conducting each one a known constant flow proportional to the potential H. The total flow is the sum of the individual flows of all active pipes and could be measured by h, where

$$h = h_\eta + (\eta - 1)H. \tag{1}$$

Thus, although h is not measured directly in a vertical stack, knowledge of η and h_η in (1) is sufficient to determine the total flow.

On the other hand, the pipes could be *horizontally stacked* as shown in Fig. 2(a).

In this case, when the potential h_j of the pipe P_j exceeds H, only the overflow fraction $f_{\mathrm{ov}(j+1)}$ is diverted to the pipe P_{j+1}, where

$$f_{\mathrm{ov}(j+1)} = W_{j+1}/(W_1 + W_2 + \cdots + W_{j+1}), \quad \text{for } 1 \leq j < n. \tag{2}$$

All the previous conducting pipes remain filling with the fraction $1 - f_{\mathrm{ov}(j+1)}$. When the last pipe becomes active, all the pipes are filling together until they become simultaneously full.

Unlike the vertical arrangement, where the maximum potential of pipe j is $h_{\max(j)} = H$, in this case

$$h_{\max(j)} = (n - j + 1)H, \qquad \text{for } 1 \leq j \leq n. \tag{3}$$

Note that this arrangement could be interpreted equivalently as being vertically stacked with pipes of height H, but with equivalent widths

$$W_{\mathrm{eq}1} = W_1 \quad W_{\mathrm{eq}(j)} = W_1 + W_2 + \cdots + W_j, \quad \text{for } 2 \leq j \leq n. \tag{4}$$

Extending the concept a little more, a hybrid arrangement could be conceived. An example of a stack of one horizontal and $n-1$ vertical pipes, here called the H^1V stack, is shown in Fig. 2(b). In this case, only pipe P_1 is permanently filling, i.e., only P_1 is filling when $h \leq H$, or the pair of P_1 and P_η is simultaneously filling when $h > H$. Thereby, (2)–(4) should be modified to

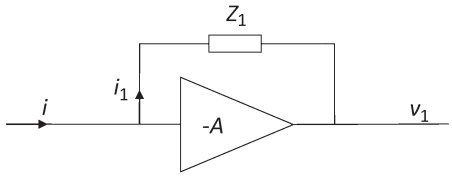

Fig. 3. Single-scale linear current arrangement.

$$f_{\mathrm{ov}(j+1)} = W_{j+1}/(W_1 + W_{j+1}), \qquad \text{for } 1 \leq j < n \tag{5}$$

$$h_{\max 1} = nH \qquad h_{\max(j)} = H, \qquad \text{for } 2 \leq j \leq n \tag{6}$$

$$W_{\mathrm{eq}1} = W_1 \qquad W_{\mathrm{eq}(j)} = W_1 + W_j, \qquad \text{for } 2 \leq j \leq n. \tag{7}$$

For all presented arrangements, the total flow is the sum of the flows of all active pipes or all pipes. Considering the last two arrangements as vertically stacked in an equivalent fashion, also, knowledge of only η and h_η $(0 \leq h_\eta \leq H)$ is sufficient to determine the total flow.

However, much more significantly, for the horizontal and hybrid stacks, the potential $h_1 = h$ of P_1 can measure directly the total flow. It can be considered as a ruler composed of a set of n linear adjacent segments (scales) that, when properly calibrated, can represent the total wide-range flow, similar to a logarithmic scale. As an example, the linear segments could be 0–1, 1–10, 10–100, 100–1000, etc. Because of this important property, the horizontal and hybrid stacks will be fully analyzed subsequently. Although not implemented in this paper, the vertical stack concept is useful to obtain equivalent and synthetic equations for the horizontal and hybrid arrangements, as will be explained in the next section.

Finally, although the maximum height has been limited to H in order to facilitate the explanation, each pipe could have any height limit, i.e., $H_1, H_2, \ldots, H_n$.

III. N-Scale OCS System

We now apply the concept of the hydraulic analogy just described for the purpose of implementing an OCS measurement system.

Let us start from a single-scale linear current system for positive input current i (entering the amplifier) as shown in Fig. 3.

Normally, Z_1 is the parallel association of a resistance R_1 with a capacitance C_1, but for the dc analysis developed in this section, $Z_1 = R_1$ is considered. Therefore, the output of this system can be written as

$$v_1 = -R_1 i_1 = -R_1 i, \qquad \text{for } v_1 \geq V_{\mathrm{fs}} \tag{8}$$

considering $V_{\mathrm{fs}} < 0$ as the full-scale voltage, $A \to \infty$, and other ideal characteristics for the amplifier block.

Let us consider $V_{\mathrm{th}1}$ $(V_{\mathrm{fs}} < V_{\mathrm{th}1} < 0)$ as a threshold voltage playing the same role of the first height H on the hydraulic analogy. To add or *stack* a new scale, the overflow current for output voltages $v_1 < V_{\mathrm{th}1}$ needs to be drained from the input

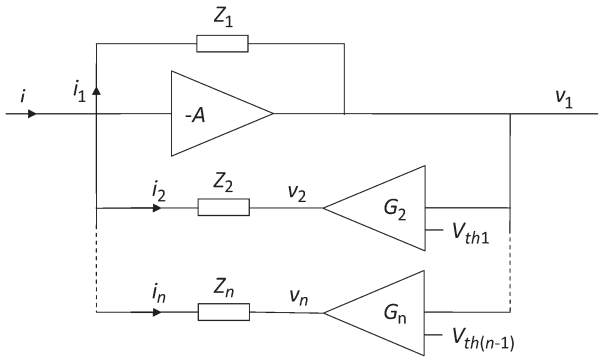

Fig. 4. N-scale OCS arrangement.

node. This can be accomplished by introducing a new loop composed of a new scaling impedance Z_2 connected to the output of an amplifier stage with gain G_2, as shown in the N-scale OCS arrangement in Fig. 4, such that

$$v_2 = G_2(v_1 - V_{\text{th1}}) \tag{9}$$

where $G_2 > 0$ for $v_1 < V_{\text{th1}}$ and $G_2 = 0$ if otherwise, corresponding to an ideal biased amplifier with a threshold V_{th1}.

In this arrangement, the impedance Z_2 is equivalent to a new stacked pipe, and the potential of the input node is equivalent to the zero height (reference level) of each pipe. By increasing the input current i, the output voltage v_1 increases proportionally in magnitude until reaching V_{th1}. If the current continues to increase, the second scale becomes active, and the output voltage v_2 starts increasing in magnitude from zero, proportionally to the overflow current i_2. Thus, the voltages v_1 and $v_2 = 0$ are not forced to change during the switching, giving practically zero switching time, independent of the impedance values Z_1 and Z_2. This is an important result because high-value scaling feedback resistances in parallel with parasitic or feedback capacitances give large time constants (e.g., $10^{11}\ \Omega//10$ pF $\rightarrow$ $\tau = 1$ s). The same above reasoning can be applied to the other stacked scales $3, 4, \ldots, n$.

Differently, in a conventional low-current switching having a scaling factor of k (e.g., $k = 10$) between two consecutive scales, long dead times would result from the forced voltage changes, V_{th} to V_{th}/k or vice versa, across large resistances. This effect could be considered undesirable, as in certain applications requiring continuous and fast response. As indicated, the OCS method eliminates this drawback.

Proceeding with the analysis of the method, we develop general equations for the arrangement in Fig. 4. In this way, (9) transforms into

$$v_j = G_j\left(v_1 - V_{\text{th}(j-1)}\right), \qquad \text{for } 2 \le j \le n \tag{10}$$

where $G_j > 0$ for $v_1 < V_{\text{th}(j-1)}$ and $G_j = 0$ if otherwise.

Also, the input current i can be calculated as

$$i = i_1 + i_2 + \cdots + i_n = -(v_1/R_1 + v_2/R_2 + \cdots + v_n/R_n) \tag{11}$$

where $Z_j = R_j \ \ (1 \le j \le n)$, for the dc analysis, was considered.

From the arrangement in Fig. 4, horizontal and hybrid stacks comprising several scales arranged as a linear wide-range ruler in v_1 can be developed.

A. Horizontal Stack

The horizontal stack is the simplest arrangement and can be implemented directly from the conditions established earlier.

As (10) does not impose any specific limit to v_j, this arrangement is analogous to the horizontal stack of pipes in Fig. 2(a), where G_j has only a multiplier effect on the scale j.

We will now derive an expression for the input current i, aiming at benefiting the further mathematical development and understanding of the method.

Interpreting this horizontal stack as equivalent to a vertical stack, the input current i can be written in a condensed form as

$$\begin{aligned} i &= I_{\text{Teq}(\eta-1)} + i_{\text{eq}(\eta)} \\ &= I_{\text{Teq}(\eta-1)} + \left[-\left(1/R_{\text{eq}(\eta)}\right)\left(v_1 - V_{\text{th}(\eta-1)}\right)\right], \\ &\qquad \text{for } V_{\text{th}(\eta)} \le v_1 \le V_{\text{th}(\eta-1)}\ (1 \le \eta \le n) \end{aligned} \tag{12}$$

where the following variables are defined.

1) η is the last active scale.
2) The constant $I_{\text{Teq}(\eta-1)}$ is the sum of the currents measured by the previous $\eta - 1$ equivalent scales already filled, i.e.,
$$I_{\text{Teq}(\eta-1)} = I_{\text{eq1}} + I_{\text{eq2}} + \cdots + I_{\text{eq}(\eta-1)} \tag{13}$$
where $I_{\text{eq}(j)} = -(1/R_{\text{eq}(j)})(V_{\text{th}(j)} - V_{\text{th}(j-1)})$ for $1 \le j < \eta$ and considering $V_{\text{th0}} = 0$ and $I_{\text{Teq0}} = 0$.
3) $1/R_{\text{eq}(\eta)}$ is the conductance of the equivalent scale η with "width" proportional to $1/R_{\text{eq}(\eta)}$ [see (4)], i.e.,
$$1/R_{\text{eq}(\eta)} = G_1/R_1 + G_2/R_2 + \cdots + G_\eta/R_\eta \tag{14}$$
considering the dummy parameter $G_1 = 1$ created for convenience.
4) $i_{\text{eq}(\eta)} = -(1/R_{\text{eq}(\eta)})(v_1 - V_{\text{th}(\eta-1)})$ is the current measured by the equivalent scale η.
5) $V_{\text{fs}} = V_{\text{th}(n)} < V_{\text{th}(n-1)} < \cdots < V_{\text{th2}} < V_{\text{th1}} < V_{\text{th0}} = 0$ are the thresholds for each scale, where $V_{\text{th}(n)}$ and V_{th0} are dummy parameters, created for convenience.

Considering the hydraulic analogy, the differences $V_{\text{th}(j)} - V_{\text{th}(j-1)}\ (1 \le j \le n)$ play the same role of the heights H (or H_j).

B. Hybrid Horizontal/Vertical Stack

In the hybrid stack, it is necessary to impose limits to the scales vertically stacked.

Let us limit v_j at $v_1 = V_{\text{th}(j)}$ for $2 \le j \le n$, by adding the following condition to (10):

$$v_j = G_j\left(V_{\text{th}(j)} - V_{\text{th}(j-1)}\right), \qquad \text{for } v_1 < V_{\text{th}(j)}. \tag{15}$$

Considering (15), the arrangement in Fig. 4 becomes analogous to the H^1V stack in Fig. 2(b).

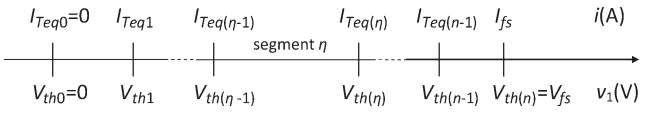

Fig. 5. Voltage v_1 of scale 1 as a ruler measuring the input current i.

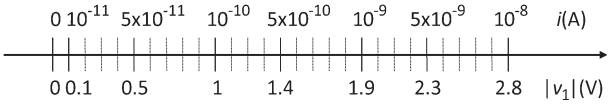

Fig. 6. Calibration example of a three-scale OCS horizontal stack.

In this arrangement, only scale 1 is permanently filling, i.e., either scale 1 is filling when $v_1 \geq V_{\rm th1}$ or the pair of scales 1 and η is simultaneously filling when $v_1 < V_{\rm th1}$.

The input current i can be calculated by (12) but considering now [see (7)]

$$1/R_{\rm eq(\eta)} = G_1/R_1 + G_\eta/R_\eta \tag{16}$$

where $1/R_{\rm eq1} = G_1/R_1$ is implied.

Finally, it is worth mentioning that the same results could be obtained with the horizontal and hybrid stacks. However, some differences should be noted between these two arrangements, such as the different numbers of feedback loops operating simultaneously and the different output limits of each scale.

IV. Processing

To obtain the input current measurement, some processing is required.

To directly process the measurement for the horizontal and hybrid stacks, the voltage v_1 of scale 1 may be considered as a ruler measuring the input current, as previously mentioned. This ruler can be composed of n adjacent linear segments (scales), similar to a logarithmic scale, but without the error originating from the logarithmic conversion process. The measurement could also be displayed on a galvanometer or a bar graph. Considering $I_{\rm fs}$ as the full-scale current corresponding to $v_1 = V_{\rm th(n)} = V_{\rm fs}$ and applying $v_1 = V_{\rm th(\eta-1)}$ in (12), a ruler of n linear segments results (Fig. 5).

In this case, R_j, G_j, and $V_{\rm th(j)}$ $(2 \leq j \leq n)$ could be properly selected in order to result in segments having the same length and appropriate ends, such as 0.1–1, 1–10, 10–100, 100–1000, etc. As an example, for a three-scale OCS horizontal stack, by setting $V_{\rm th1} = -1$ V, $V_{\rm th2} = -1.9$ V, and $V_{\rm th3} = -2.8$ V, making $G_1 = G_2 = G_3 = 1$, and selecting $R_1 = 10^{10}$ Ω, $R_2 = (10^{10}/9)$ Ω, and $R_3 = (10^{10}/90)$ Ω to result in $R_{\rm eq1} = 10^{10}$ Ω, $R_{\rm eq2} = 10^9$ Ω, and $R_{\rm eq3} = 10^8$ Ω, from (12), the ruler composed of three linear segments results calibrated as shown in Fig. 6. Here, the first segment $0 \leq |v_1| \leq 1$ V was made larger in order to include the initial subinterval [0, 0.1] V corresponding to [0, 10^{-11}] A.

In addition, this calibration provides a scaling factor of ten between two adjacent equivalent scales, i.e., a range of $\Delta v_1 = 100$ mV corresponds to 10^{-11}, 10^{-10}, and 10^{-9} A, in the corresponding equivalent scales 1, 2, and 3.

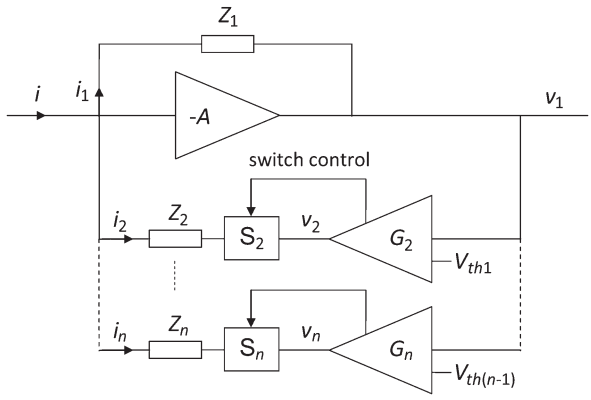

Fig. 7. Arrangement of analog switches S_j $(2 \leq j \leq n)$ to reduce the effect of leakage current on the lower scales.

Consider now the above example as a three-scale OCS hybrid $\rm H^1V$ stack. By modifying only R_3 to $(10^{10}/99)$ Ω, the same results are obtained.

On the other hand, using an analog-to-digital converter arrangement, many alternatives are possible. As an example, from the acquisition of v_1 and considering (12), the input current can be calculated by a simple algorithm resident in a microcontroller system.

Finally, it should be mentioned that, although the vertical stack has not been completely addressed in this text, by simply adding its scales outputs, i.e., $v_1 + v_2 + \cdots + v_n$, a similar ruler like that presented for the horizontal and hybrid stacks could be built.

In short, there are many possibilities to process the OCS measurement.

V. Design Considerations

In this section, certain considerations for a real implementation of an OCS system are addressed.

A. Leakage Currents and Switching

Let us consider the case of a five-scale $(n = 5)$ OCS system with a range of 10^{-11}–10^{-6} A. The corresponding range of feedback resistances could be 10^{10} to $10^7/9$ Ω, i.e., 100 mV represents 10^{-11} A in the first scale.

Also, real operational amplifiers having offset voltages, related drifts, and finite open-loop gains should be considered. Let $V_{r(j)}$ be the residual voltage drop on the feedback resistance R_j $(2 \leq j \leq n)$ as a result of these limited characteristics. If, for example, $|V_{r5}|$ reaches 1 mV on the $(10^7/9)$ Ω feedback resistance, a 0.9-nA leakage current will result and disturb the input node. This would render the use of the two lower scales impractical.

A solution for this problem is to stack each next scale up only when it becomes active. This can be performed by including an analog switch S_j $(2 \leq j \leq n)$ in the feedback path of each scale, as shown in Fig. 7. The control of these switches can be performed by adding a comparator to each biased amplifier, in order to indicate when the corresponding scale is active.

Let us further analyze the concept shown in Fig. 7. A practical design depends on certain particularities, such as

the minimum current to be measured, the number of scales, the characteristics of the switches, and the accuracy required. Using the aforementioned example of a five-scale ($n = 5$) OCS system with a range of 10^{-11}–10^{-6} A, consider in addition switches with off, on, and isolation resistances of $r_{\rm off} = 300$ MΩ, $r_{\rm on} = 200$ Ω, and $r_{\rm iso} > 10^{11}$ Ω, respectively. When the first scale is active, the four upper inactive scales could inject in the input node a leakage current around 10 pA for $|V_{r(j)}| = 1$ mV. Therefore, it is necessary to particularize the basic concept in Fig. 7 in order to obtain better results. A solution can be to consider each S_j as a more elaborated switch arrangement. A "T" topology arrangement, i.e., with series–shunt–series ($\mathsf{s_a}-\mathsf{sh}-\mathsf{s_b}$) switches, can be used. Switch $\mathsf{s_a}$ is connected to the feedback resistance, sh to the ground, and $\mathsf{s_b}$ to the biased amplifier output. This arrangement, when in the OFF state (off–on–off), connects the feedback resistance in series with $r_{\rm off} + r_{\rm on}$ to the ground of the input node and also reduces the residual output voltage of the biased amplifier to a fraction close to $r_{\rm on}/r_{\rm off}$. On the other hand, when in the ON state (on–off–on), the scale is activated by the feedback resistance in series with $2r_{\rm on}$, and the shunt resistance $r_{\rm off}$ is connected to the biased amplifier output via $r_{\rm on}$.

It is important to note that, by providing a good grounding, this procedure practically eliminates the (dc+ac) influence, of the biased amplifier output of an inactive scale, on $V_{r(j)}$. Therefore, before stacking the scale j, $V_{r(j)}$ is normally a fraction of the input node voltage v_0, and the resulting leakage current becomes easier to compensate. Also, considering signal variations (see stability in Section V-B), the noise analysis of the arrangement becomes similar to that of a conventional n-scale system, since any possible disturbance coming from an inactive scale is minimized, as implied earlier.

Proceeding with the example, it is appropriate to consider the shunt effect of the resistance near $(R_j + r_{\rm off})/4$ (> 75 MΩ) in the input node. This results from the parallel association of the off equivalent resistances of the four upper inactive scales. Low values of the resulting resistance increase the offset voltage gain and the noise voltage gain of the input amplifier. In order to reduce this effect, among other solutions, it is possible to almost double this resistance by inserting one more series switch $2\mathsf{s_a}-\mathsf{sh}-\mathsf{s_b}$ in each feedback path. In certain cases, for scales of higher current (e.g., 1 mA), it is necessary to take into account the accuracy of the total contribution of $r_{\rm on}$ included in the feedback resistance of each scale. This could force to adopt other procedures for correcting this effect.

It is worth mentioning that a more simplified switch arrangement $\mathsf{s_a}-\mathsf{sh}-\mathsf{s_b}$, where switch $\mathsf{s_b}$ is replaced by a simple series resistance R_s ($R_s \gg r_{\rm on}$), can be appropriate in certain cases. Its operation and analysis are quite similar to those described earlier.

In short, although there is not a single detailed solution for all cases, the basic arrangement in Fig. 7 reduces the effect of leakage current on the lower scales.

From the standpoint of switching, we consider that any capacitance C_j in parallel with R_j ($2 \le j \le n$) is minimized to a low residual value. For worst case transient and error analysis in certain practical conditions, it can be considered that, during the stacking of the scale j, the change in $|V_{r(j)}|$ imposes a corresponding step to v_1 not greater than $|V_{r(j)}|$. In this case, $|V_{r(j)}| \le |v_0| + |v_j|$, where v_j is replaced by its residual value before the switching. Also, after the switching, any leakage current coming from the control terminal is drained by the path connected to the low-impedance output of the biased amplifier. Thus, the expected transient amplitude in v_1 is limited in $|V_{r(j)}|$, even in the case that the $V_{r(j)}$ sign results in draining the current from the input node, when oscillation occurs during the commutation.

The effect of any charge injection has to be negligible for the above reasoning to be valid. To guarantee this condition, a photocoupled FET switch can be used. This type of device has zero channel charge injection, and only its feedthrough gate injection through very low capacitances (e.g., 0.2 pF) should be considered. This last effect results in small spikes in the transitions, which can be minimized by a good design.

Finally, the above discussion aims at highlighting some of the problems involved in an OCS design. As a result, high-precision operational amplifiers having mainly low offset voltage should be used in the loop path. Also, besides using switches with similar or even better characteristics than those above described, a careful design providing good grounding and also shielding techniques should be considered.

B. Time Response and Stability

In low-current applications where a random signal is to be measured, an OCS system should have sufficient measurement time or integration time in its scales in order to have appropriate relative statistical fluctuation (standard deviation/|mean|) in the entire range. As the measurement time determines the time response behavior of the system, this tradeoff should be managed.

Let us now consider the n-scale OCS system in Fig. 4. The bandwidth of the biased amplifiers is wide enough for not introducing important phase shift in the loops, so that it is possible to assume G_j ($2 \le j \le n$) as a simple scalar or a scaling factor. Thus, for the purpose of evaluating the response time of the n-scale OCS system, if the arrangement is operating in the scale η and all variables are represented as variations in the Laplace transform domain, the closed-loop transfer function can be approximated to

$$G_{c(\eta)} = v_1/i = R_{\mathrm{eq}(\eta)}/\left(1 + s\tau_{\mathrm{eq}(\eta)}\right) \tag{17}$$

where $Z_j = R_j//C_j$ ($1 \le j \le \eta$) and $\tau_{\mathrm{eq}(\eta)} = R_{\mathrm{eq}(\eta)}C_{\mathrm{eq}(\eta)}$ were considered. For a horizontal stack, $R_{\mathrm{eq}(\eta)}$ is defined as that in (14), and $C_{\mathrm{eq}(\eta)} = C_1G_1 + C_2G_2 + \cdots + C_\eta G_\eta$. For a hybrid $\mathrm{H^1V}$ stack, $R_{\mathrm{eq}(\eta)}$ is defined as that in (16), and $C_{\mathrm{eq}(\eta)} = C_1G_1 + C_\eta G_\eta$. Normally, C_j ($2 \le j \le n$) is minimized as already mentioned. Therefore, for $C_j \ll C_1$ and G_j close to one, $C_{\mathrm{eq}(\eta)} \approx C_1$ results.

In (17), $\tau_{\mathrm{eq}(\eta)}$ defines the time response of the arrangement when η scales are active.

From the standpoint of stability, the main concern is to make the bandwidth of each biased amplifier wide enough, to keep the introduced phase shift $\Delta\varphi$ as low as possible and thus assuring appropriate phase margin for stability. When many loops are in operation, considering $G_j = 1$ ($2 \le j \le n$), the

feedback paths are equivalent, for signal variations, to only one biased amplifier connected to the parallel association of the corresponding feedback impedances. Therefore, by reducing $\Delta\varphi$, the arrangement approximates to the stable single-scale configuration shown in Fig. 3.

On the other hand, it is possible to demonstrate that stability can also be assured considering more detailed issues, such as the existence of an input coaxial cable, among others.

C. Accuracy

A worst case accuracy analysis was performed in order to estimate the limits of the method.

From (12) and considering $G_j = 1$, it is easy to see that three types of parameters affect the accuracy of the measured input current i: the residual voltages $V_{r(j)}$, because they affect v_1 (see switching in Section V-A), the threshold voltages $V_{\mathrm{th}(j)}$, and the feedback resistances R_j (components of $R_{\mathrm{eq}(j)}$). The concept of $V_{r(j)}$ is extended in order to include $j = 1$ (V_{r1}), i.e., the residual output voltage of the input amplifier resulting from the leakage current in the input node and any eventual offset.

Let us define k_j $(2 \le j \le n)$ as the ratio $I_{\mathrm{Teq}(j)}/I_{\mathrm{Teq}(j-1)}$ of current boundaries of the equivalent scale j (see Fig. 5), and $k_1 = I_{\mathrm{Teq1}}/I_{\min}$, where $I_{\min}$ is the minimum current to be measured. Considering the practical case where $k_j \gg 1$ (e.g., $k_j = 10$), the following approximation results for $2 \le j \le n$:

$$I_{\mathrm{Teq}(j)} \approx I_{\mathrm{eq}(j)} = -\left(1/R_{\mathrm{eq}(j)}\right)\left(V_{\mathrm{th}(j)} - V_{\mathrm{th}(j-1)}\right). \quad (18)$$

In this case, from (12), the relative error $\delta i/i$ of the measured input current i can be estimated at the beginning ($v_1 = V_{\mathrm{th}(\eta-1)+}$) and at the end ($v_1 = V_{\mathrm{th}(\eta)-}$) of the equivalent last active scale η $(1 \le \eta \le n)$ as

$$\varepsilon_{b(\eta)} = (\delta i/i)|_{v_1 = V_{\mathrm{th}(\eta-1)+}} \approx \varepsilon_{e(\eta-1)} + k_\eta \left[\delta V_{0(\eta)} / \left|\Delta V_{\mathrm{th}(\eta)}\right|\right] \quad (19)$$

$$\varepsilon_{e(\eta)} = (\delta i/i)\,\big|_{v_1 = V_{\mathrm{th}(\eta)-}} \approx \varepsilon_{b(\eta)}/k_\eta + \delta\Delta V_{\mathrm{th}(\eta)} / \left|\Delta V_{\mathrm{th}(\eta)}\right| + \delta R_{\mathrm{eq}(\eta)}/R_{\mathrm{eq}(\eta)} \quad (20)$$

where the following variables are defined.

1) $\varepsilon_{b(\eta)}$ and $\varepsilon_{e(\eta)}$ are the relative errors of the measured current i (where b stands for beginning and e stands for end) of the equivalent scale η. For $\eta = 1$, $\varepsilon_{e0} = 0$.
2) $\delta V_{0(\eta)}$ is the error associated with the term $v_1 - V_{\mathrm{th}(\eta-1)}$ in (12) at the beginning of the equivalent scale η. For $\eta \ge 2$, $\delta V_{0(\eta)} = |V_{r(\eta)}| + \delta V_{\mathrm{th}(\eta-1)}$ results, where $\delta V_{\mathrm{th}(\eta-1)}$ is the error of the threshold $V_{\mathrm{th}(\eta-1)}$. For $\eta = 1$, δV_{01} is the magnitude of the residual output voltage v_1 resulting from the input node leakage current and from any offset of the input amplifier.
3) $\Delta V_{\mathrm{th}(\eta)} = V_{\mathrm{th}(\eta)} - V_{\mathrm{th}(\eta-1)}$, and $\delta\Delta V_{\mathrm{th}(\eta)}$ is its associated error.
4) $\delta R_{\mathrm{eq}(\eta)}$ is the error of $R_{\mathrm{eq}(\eta)}$. For $k_\eta \gg 1$, as in many cases, $R_{\eta-1} \gg R_\eta$; then, $R_{\mathrm{eq}(\eta)} \approx R_\eta$, and $\delta R_{\mathrm{eq}(\eta)}/R_{\mathrm{eq}(\eta)} \approx \delta R_\eta/R_\eta$.

In general, using low-tolerance feedback resistors, the relative error is higher at the beginning of the scale, where it is defined practically by the term $k_\eta[\delta V_{0(\eta)}/|\Delta V_{\mathrm{th}(\eta)}|]$ in (19). As a result, normally, the relative error presents a sawtooth behavior along the entire range, i.e., a downward slope from $\varepsilon_{b(\eta)}$ to $\varepsilon_{e(\eta)}$ in the corresponding interval $[I_{\mathrm{Teq}(\eta-1)}, I_{\mathrm{Teq}(\eta)}]$. As an example, considering $\eta \ge 2$, $\varepsilon_{e(\eta-1)} = 0.01$, $k_\eta = 10$, $V_{r(\eta)} = \delta V_{\mathrm{th}(\eta-1)} = \delta\Delta V_{\mathrm{th}(\eta)} = 2$ mV, $\Delta V_{\mathrm{th}(\eta)} = 2$ V, and $\delta R_{\mathrm{eq}(\eta)}/R_{\mathrm{eq}(\eta)} = 0.01$, the relative errors $\varepsilon_{b(\eta)} \approx 0.03$ (3%) and $\varepsilon_{e(\eta)} \approx 0.014$ (1.4%) result.

Considering the threshold voltages, current technology provides high-precision voltage references (e.g., 0.02%, 1 ppm/°C) and low-tolerance resistors (e.g., 0.01%, 10 ppm/°C). Also, considering voltage offsets, high-precision operational amplifiers with low offset (e.g., < 100 μV, 1 μV/°C) are today available. Therefore, the contribution of the corresponding errors can be minimized in a practical case.

Other OCS design considerations could be addressed. However, most of them are common to the design of electrometer devices and could be found, for example, in [8], [11], and [12].

VI. Simulation

Several computer simulations using a SPICE program have been performed. As a typical example, a five-scale horizontal OCS system with a range of 10^{-11} to 2×10^{-6} A was designed and simulated, closely following the above indications.

The feedback impedance Z_1 was set at 10^{10} $\Omega//100$ pF. The feedback resistances R_2 to R_5 were set at $(10^{10}/9)$ to $(10^7/9)$ Ω, with the contribution of the resistances of their switch arrangements included. Only parasitic capacitances of 0.2 pF were considered for C_2 to C_5. The voltage thresholds $V_{\mathrm{th}(j)}$ $(1 \le j \le 4)$ were set at -2, -3.8, -5.6, and -7.4 V. A range of 1.8 V was allowed for the last scale, so that -9.2 V $\le v_1 \le 0$. Also, $G_j = 1$ $(2 \le j \le 5)$. Thus, a full-scale input current of 2 μA resulted.

A $2\mathsf{s_a}{-}\mathsf{sh}{-}\mathsf{s_b}$ (previous nomenclature) switch arrangement was designed for the four upper scales, where the element in series $\mathsf{s_b}$ is a resistance $R_s = 20$ kΩ. A photocoupled FET, with turn-on and turn-off times of 15 μs, a capacitance between the two signal terminals of 15 pF, and other characteristics already mentioned in Section V, was used as the basic switch device. The input amplifier was built with a very low bias current and low-offset-voltage operational amplifier. An offset adjustment circuit was provided to cancel any residual offset on the first scale. A biased amplifier module (Fig. 8) having a comparator for switch control, based mainly on wide-bandwidth and low-offset-voltage operational amplifiers, was designed. The quasi-ideal diode (D_2, U_3) provides the nonlinear characteristic of the biased amplifier.

The outputs of all the scales were filtered ($\tau = 1$ ms) in order to eliminate any eventual high-frequency transient, also limiting the minimum response time of the faster scales to this value. In order to evaluate the real performance of the method, no attempt to optimize the circuit was effected.

An input coaxial cable with a lumped impedance of 10^9 $\Omega//1$ nF and a series input resistance of 1 kΩ was considered.

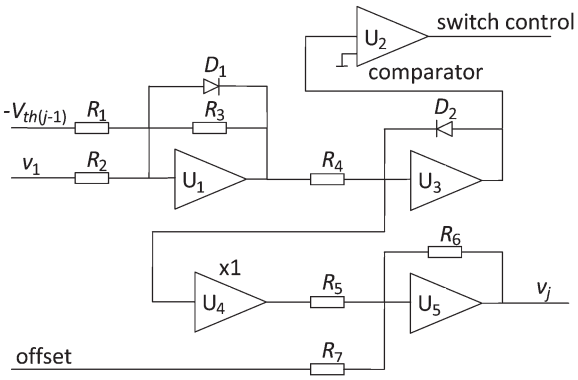

Fig. 8. Basic topology of the biased amplifier module.

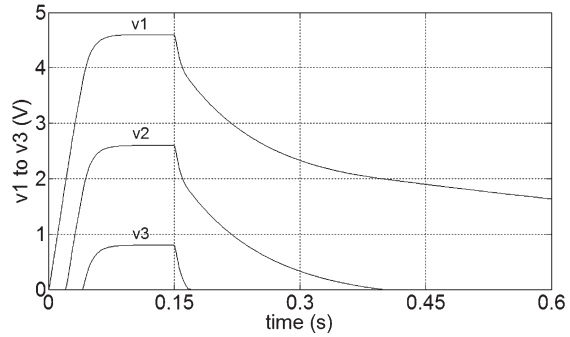

Fig. 9. Response to a trapezoidal (10 μs/150 ms/10 μs) input current transient of range [0, 10^{-8}] A, crossing the boundaries between scales 1, 2, and 3.

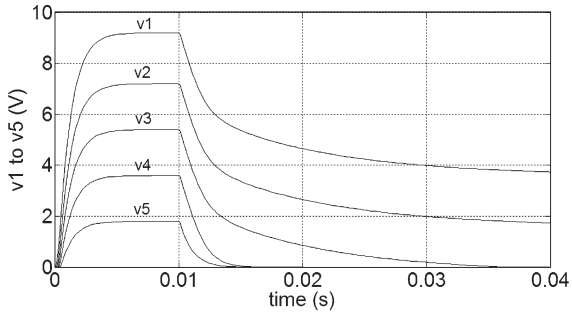

Fig. 10. Response to a full-range [0, 2×10^{-6}]-A trapezoidal (10 μs/ 10 ms/10 μs) input current transient.

The circuit was submitted to steady-state and transient tests simulating input current values in the entire range. The outputs were monitored, and the measured input current was processed by (12). Some results are presented in the following.

As all voltages v_j and $V_{\mathrm{th}(j)}$ $(1 \leq j \leq 5)$ are negative, the presentation of the results and their analysis were performed in magnitude in order to improve the understanding, so that, from this point on, all negative signs of these variables have been discarded.

For the following three transient tests shown in Figs. 9–11, no errors in the parameters of the circuit were imposed.

A trapezoidal (10 μs/150 ms/10 μs) current transient of range [0, 10^{-8}] A, crossing the boundaries between scales 1, 2, and 3, was applied to the input. Fig. 9 shows the output voltage responses v_1, v_2, and v_3. When the rising edge of v_1 crosses the thresholds $V_{\mathrm{th1}} = 2$ V $(2 \times 10^{-10}$ A) and $V_{\mathrm{th2}} = 3.8$ V $(2 \times 10^{-9}$ A), the outputs v_2 and v_3 start increasing from zero, respectively, all in a continuous and smooth way.

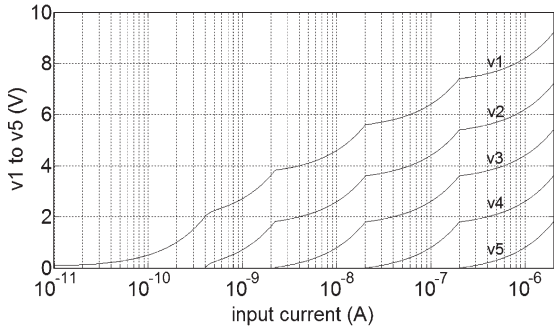

Fig. 11. Response to a full-range $[10^{-11}, 2 \times 10^{-6}]$-A exponential input current transient having a period of 1 s. The total excursion time is 12.2 s.

The v_1 rise time (0%–90%) is less than 50 ms, and the relative deviation of the measured current at the end of the pulse is better than 0.1%. On the falling edge, as each threshold is crossed, the time constant of v_1 is switched, from approximately 10 ms to 100 ms and 1 s, respectively. No effect of the switches S_2 and S_3 operation is perceptible.

In the sequence, a full-range [0, 2×10^{-6}]-A trapezoidal (10 μs/10 ms/10 μs) input current transient was applied to the input. Fig. 10 shows the responses v_1, v_2, v_3, v_4, and v_5. Note that, in this case, the filter ($\tau = 1$ ms), included at each output, now limits the rise time. Therefore, the starting rise of each scale voltage at each threshold is no more visible. The rise time is less than 3 ms, and the relative deviation of the measured current at the end of the pulse is also better than 0.1%. As the fall times are also limited by the filter, the last faster scales (4 and 5) fall practically together.

Then, a full-range $[10^{-11}, 2 \times 10^{-6}]$-A exponential current transient of type $i = I_0 \exp(t/T)$, with a period T of 1 s, has been applied to the input. Fig. 11 shows the responses v_1, v_2, v_3, v_4, and v_5. As the range is composed of linear decades, a quasi-linear behavior similar to a log scale is visible.

The responses to these transients show the dynamic characteristics of the method. Note that the time response behavior is only limited by the design parameters and not intrinsically by the method. Also, at this level of analysis, continuous and smooth evolutions are clearly visible. However, to obtain a deeper view of the accuracy of the method, an evaluation of the relative error of the measured input current, when errors in the parameters of the circuit are present, is needed. Thus, a static test evaluating the real accuracy in all the range and a dynamic one highlighting the tradeoff between accuracy and time response have been performed. For that, the following errors were inserted in certain parameters of the circuit: 1) The leakage current in the input node was not compensated; 2) the output offset voltages of the biased amplifiers were set at $v_2 = 1$ mV, $v_3 = 2$ mV, $v_4 = 3$ mV, and $v_5 = 5$ mV; 3) a relative error of $\delta\Delta V_{\mathrm{th2}}/\Delta V_{\mathrm{th2}} = 0.005$ (0.5%) was added to the threshold V_{th2}; and 4) relative errors of $\delta R_2/R_2 = \delta R_3/R_3 = 0.01$ (1%) and $\delta R_5/R_5 = 0.005$ (0.5%) were imposed to the feedback resistances. Except for δR_5, all errors were added to their parameters.

For static measurements in points distributed in the entire range and for the response to the exponential transient described previously, the relative error (in percent) of the measured input current was calculated for the entire range, as shown in Fig. 12.

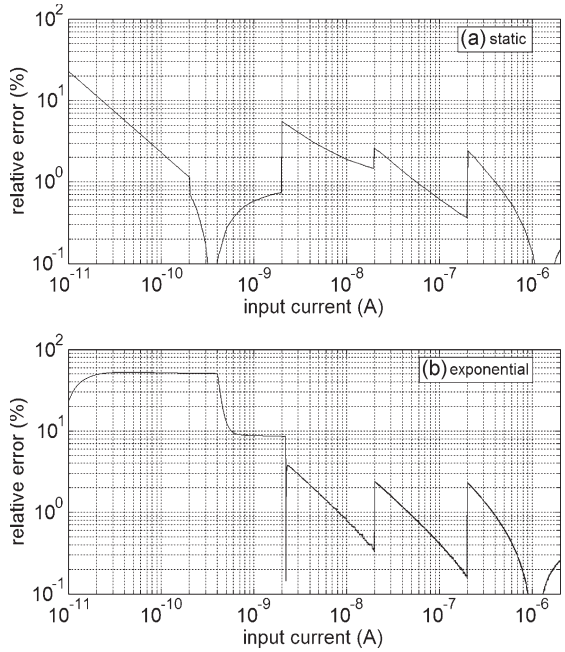

Fig. 12. Relative error (in percent) of the measured current for a full-range $[10^{-11}, 2 \times 10^{-6}]$-A input calculated in two cases: (a) For static measurements in points distributed in the range and (b) for the response to an exponential transient having a period of 1 s. Errors were inserted: Leakage current in the input node, output offset voltages of $v_2 = 1$ mV, $v_3 = 2$ mV, $v_4 = 3$ mV, and $v_5 = 5$ mV, and relative errors of $\delta\Delta V_{\rm th2}/\Delta V_{\rm th2} = 0.005$ (0.5%), $\delta R_2/R_2 = \delta R_3/R_3 = 0.01$ (1%), and $\delta R_5/R_5 = 0.005$ (0.5%). Except for δR_5, all errors were added to their parameters.

The static test shows a decreasing contribution of the leakage current (< 3 pA) drained from the input node, for the relative error in scale 1. In scale 2, the combination of the offset voltage v_2 and the higher value of R_2 performs some compensation of the leakage current. At the end of the scale, the relative error approximates to the error in R_2. At the beginning of scale 3, the effects of the offset voltage v_3 and of $\delta\Delta V_{\rm th2}/\Delta V_{\rm th2}$ step up the relative error above 5%. The error value of R_3 explains the negative slope in this scale. At the beginning of scale 4, the contribution of the offset voltage v_4 increases the relative error again, and the negative slope in the scale remains constant as a result of the exact value of R_4. For scale 5, $v_5 = 5$ mV provides a greater step at the beginning of the scale, and the lower value of R_5 provides some compensation. It is worth noting the sawtooth behavior of the relative error along the range, already referred to.

For the response to the exponential transient, the relative error is a combination of the static error with the deviation caused by the response time of each scale. It reaches a maximum close to 53%, slightly increased by the leakage current, and 4.25 s (7×10^{-10} A) after the start of the transient, it is near to 9%. The first decrease occurs with some delay after the first scale switching (1–2) at 2×10^{-10} A, while the second is closer to the next threshold at 2×10^{-9} A as a result of the short time constant of 10 ms in this region. In faster scales 3, 4, and 5, the response follows better the input, and the relative error more closely approximates the static error, although some delay still occurs.

In short, the response follows the input according to the time constants set in the design. The faster the scale, the smaller is the relative error until it approaches the limit set by the errors in the parameters.

The results obtained above reinforce the need to use high-precision devices and the need to provide a good grounding in the design of an OCS system.

Finally, the operational amplifiers were replaced by others from different manufacturers, and similar results were obtained. Also, a five-scale hybrid H^1V OCS system simulation showed a similar performance.

VII. Conclusion

A new method to switch current for linear wide-range measurement systems has been proposed. A system using this approach behaves as a logarithmic one but retains the benefits of linear segmented scales. Several computer realistic simulations in SPICE demonstrated the viability of the technique, anticipating that a physical implementation can be obtained with current technology. The simulated results showed a continuous, smooth, and fast response in the entire range, still holding suitable accuracy for many applications.

Certainly, the OCS method requires a more elaborate design, mainly for the feedback paths, than those normally used for a conventional switching method. Today, however, high-quality devices, particularly high-precision, low-current, low-noise, and fast operational amplifiers, are available. In addition, current technology offers the possibility to build compact high-quality assemblies, thus minimizing undesirable disturbances. Therefore, the design issue should not be a constraint. Without any further processing, the output representing the measured input current could be displayed directly like a ruler in an old galvanometer, and also, using a simple algorithm, the output could be processed by modern microcontroller systems.

Although it has been originally conceived for nuclear applications, the method is quite general and can be applied to other fields, in order to develop fast and continuous linear wide-range measurement systems.

Acknowledgment

The authors would like to thank the editors and reviewers of the IEEE Transactions on Instrumentation and Measurement for their contribution to the completion of this paper. Their comments and suggestions were very helpful for improving its initial version.

References

[1] M. N. Ericson, K. G. Falter, and J. M. Rochelle, "A wide-range logarithmic electrometer with improved accuracy and temperature stability," *IEEE Trans. Instrum. Meas.*, vol. 41, no. 6, pp. 968–973, Dec. 1992.

[2] S. Shaw, "An integrated-circuit based wide range electrometer implemented with automatically ranged linear display," *Rev. Sci. Instrum.*, vol. 63, no. 6, pp. 3505–3507, Jun. 1992.

[3] S. S. Rajput and S. C. Garg, "A high resolution autogain ranging linear electrometer amplifier," *Rev. Sci. Instrum.*, vol. 67, no. 2, pp. 609–611, Feb. 1996.

[4] S. Shaw and R. Chang, "A novel wide range electrometer with quasilinear output," *Rev. Sci. Instrum.*, vol. 68, no. 10, pp. 3917–3919, Oct. 1997.

[5] Y. Acharya, "A wide range linear electrometer," *Rev. Sci. Instrum.*, vol. 71, no. 6, pp. 2585–2588, Jun. 2000.

[6] J. M. Harrer and J. G. Beckerley, *Nuclear Power Reactor Instrumentation Handbook*. Washington, DC: U.S. Atomic Energy Commission, 1973.
[7] M. T. Khaleeq, I. Zaka, H. Qaiser, B. H. Nayyar, I. A. Ghumman, and A. Ali, "A new wide-range reactor power-measuring channel," *IEEE Trans. Nucl. Sci.*, vol. 50, no. 6, pp. 2445–2451, Dec. 2003.
[8] R. W. J. Barker, "Modern electrometer techniques," *Proc. Inst. Elect. Eng.*, vol. 126, no. 11, pp. 1053–1068, Nov. 1979.
[9] N. R. Campbell and V. J. Francis, "A theory of valve and circuit noise," *J. Inst. Elect. Eng.*, vol. 93, pt. III, no. 21, pp. 45–52, 1946.
[10] W. R. Fletcher, "Wide-Dynamic Range Electrometer With a Fast Response," U.S. Patent Appl. Publ. 2011/0012588 A1, Jan. 3, 2011.
[11] *Low Level Measurements Handbook—Precision DC Current, Voltage, and Resistance Measurements*, 6th ed. Cleveland, OH: Keithley Instrum. Inc., 2004.
[12] R. Morrison, *Grounding and Shielding Techniques*, 4th ed. New York: Wiley-Interscience, 1998.

Eduardo Winston Pontes received the B.S.E.E. degree and the Ph.D. degree in nuclear science technology from the Universidade de São Paulo (USP), São Paulo, Brazil, in 1974 and 1997, respectively.

Since 1975, he has been with the Instituto de Pesquisas Energéticas e Nucleares (IPEN), Comissão Nacional de Energia Nuclear, São Paulo, at USP, where he is a Senior Research Engineer. From 1988 to 1990, he was with Merlin Gerin, Grenoble, France, where he worked in the design of a nuclear instrumentation system for a research reactor. His technological achievements include the development of several electronic systems for IPEN and the Brazilian Navy. He also currently lectures graduate courses at the Departamento de Engenharia de Telecomunicações e Controle, USP. His main research interests are in nuclear science technology, instrumentation, and signal processing.

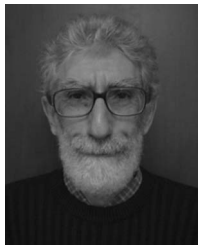

Ademar Ferreira (M'94) received the B.S.E.E. degree, the Ph.D. degree in electrical engineering, and the B.A. degree in philosophy from the Universidade de São Paulo (USP), São Paulo, Brazil, in 1964, 1969, and 1988, respectively.

In 1971/1972, he was a Doctoral Fellow with the Department of Electrical Engineering, Stanford University, Stanford, CA. Since 1999, he has been an Associate Professor with the Departamento de Engenharia de Telecomunicações e Controle, USP, where he currently leads a research group in robotics and cognitive science and technology at USP. His research interests include signal processing, systems engineering, instrumentation, and, lately, embodied cognitive robotics.